Title:

Integrating biodiversity, structural complexity, and canopy dynamics across a national forest gradient in Bhutan: Implications for monitoring and management

Running title

Biodiversity and structure across a national forest gradient

Authors:
Wangdi[a]*, Laxmi Sagar[b], Sangay Chedup[c], Sangay Dorjee[d], Tashi Waiba Norbu[e]

[ade]Forest Resources Planning & Management Division, Department of Forests and Park Services, Ministry of Energy and Natural Resources, Royal Government of Bhutan, Thimphu, Bhutan
[b]College of Natural Resources, Royal University of Bhutan. Lobesa, Punakha
[c]Divisional Forest Office, Mongar, Department of Forests and Park Services, Ministry of Energy and Natural Resources, Royal Government of Bhutan, Thimphu, Bhutan

Corresponding Author
*Wangdi
Email: wangdiues@gmail.com
Phone: +975-17506599

ORCID IDs
Wangdi: https://orcid.org/0009-0007-7726-1742
Laxmi Sagar: https://orcid.org/0000-0002-9788-6770
Sangay Chedup: https://orcid.org/0009-0008-2018-6435
Sangay Dorjee: https://orcid.org/0009-0004-9566-9133
Tashi Norbu Waiba: https://orcid.org/0009-0000-3159-2107

Manuscript Details

- **Article type:** Regular Paper
- **Main figures:** 9 (Figs. 1–9)
- **Supplementary figures:** 2 (Figs. S1–S2)
- **Tables:** 4 (Tables 1–4)
- **Supplementary tables:** 4 (Tables S1–S4)
- **Supplementary methods:** 5 (SM1–SM5)
- **References:** 37

Abstract

Climate-driven range shifts and uneven anthropogenic pressures are restructuring mountain forests globally, yet management-ready baselines rarely integrate field inventories, community ecology, structural metrics, and long-term remote sensing across full elevational gradients. Here, we use Bhutan's mountain forest system as a representative high-biodiversity Himalayan landscape, linking vegetation records from 1,942 National Forest Inventory (NFI) plots with environmental rasters and MODIS products. We quantified alpha diversity, community turnover, constrained ordination, indicator species, co-occurrence structure, a composite Stratification Complexity Index (SCI), and Enhanced Vegetation Index (EVI) trends (2000–2024).

The cleaned dataset comprised 107,876 records and 2,185 species. Mean plot richness was 17.09 ± 9.13 species (range 1–57), peaking at 500–1,000 m and declining above 4,000 m (Kruskal–Wallis $H = 630.8$, $p < 0.001$, $\varepsilon^2 = 0.322$). Forest type explained a modest proportion of compositional variation (PERMANOVA $R^2 = 0.089$, $p = 0.001$; ANOSIM $R = 0.356$), while canonical correspondence analysis identified temperature–elevation and precipitation gradients as dominant environmental axes (adjusted $R^2 = 0.042$). Indicator analysis revealed 162 significant species–forest-type associations after false discovery rate correction. Co-occurrence network modularity exceeded null expectations but with low effect size ($Q = 0.3296$; SES = 1.415, $p = 0.01$), indicating weak non-random structure. SCI was highest in low-elevation broadleaved forests and lowest in alpine scrub. Pixel-level analysis showed 29.86% of Bhutan exhibiting significant greening after multiple-testing correction, but plot-level EVI trends were only weakly correlated with richness ($\rho = 0.126$) and SCI ($\rho = 0.097$).

These results demonstrate that biodiversity, structural complexity, and canopy dynamics are only weakly coupled across mountain gradients. Low-elevation forests concentrate both diversity and structural complexity while remaining exposed to anthropogenic pressures. Satellite-derived greenness captures canopy dynamics but is not a reliable proxy for floristic or structural change. The integrated inventory–remote sensing workflow provides a transferable, reproducible framework for multi-indicator monitoring of climate-sensitive mountain ecosystems.

Keywords

canonical correspondence analysis; co-occurrence network; Eastern Himalaya; indicator species; MODIS EVI; species richness; stratification complexity index

1. Introduction

Climate-driven range shifts and uneven human pressure are reorganizing mountain forests worldwide, but monitoring systems still struggle to resolve how species diversity, community turnover, structural complexity, and canopy condition change together along steep environmental gradients. This challenge is especially acute in mountain biodiversity hotspots, where strong climatic turnover is compressed into short horizontal distances and elevation-dependent warming can rapidly redistribute ecological zones (Myers et al., 2000; Mountain Research Initiative EDW Working Group, 2015; Körner, 2007; McCain, 2009). Altitudinal corridors therefore provide model systems for understanding how environmental filtering and management pressure interact in climate-sensitive forests.

Despite extensive work on elevational diversity patterns, integrated monitoring approaches that jointly analyse inventory data, multivariate community structure, vegetation complexity, and long-term satellite trends within a single reproducible workflow remain uncommon (Pereira et al., 2013; Skidmore et al., 2021; Cavender-Bares et al., 2022). That integration is necessary because richness, turnover, vertical complexity, and greenness do not necessarily respond in parallel to the same drivers. A monitoring framework that evaluates these dimensions jointly is more informative for adaptive forest management than any single biodiversity or remote-sensing metric considered in isolation.

The study area is informative within this broader context not merely as a geographic location, but as a representative mountain system within the Eastern Himalaya. The analysis is based on a Bhutan-wide National Forest Inventory, encompassing plots spanning 113–5,469 m in elevation. Across this full national extent, the inventory captures a wide spectrum of vegetation types, including subtropical broadleaved forests, temperate broadleaved forests, conifer forests, alpine scrub, and non-forest categories within a relatively continuous mountain landscape (Wangda & Ohsawa, 2006). This combination of steep climatic compression, pronounced floristic turnover, and management-relevant forest heterogeneity reflects conditions characteristic of many mountain regions, where conservation priorities, resource use, and climate adaptation must be addressed concurrently.

Using Bhutan-wide NFI vegetation records linked to environmental rasters and MODIS time series, we applied a reproducible Python-based workflow to quantify alpha diversity, beta diversity, constrained ordination, indicator species, co-occurrence structure, a composite Stratification Complexity Index (SCI), and greenness trends over 2000–2024. This integrated design permits assessment of whether plot-level diversity, community turnover, structural complexity, and canopy greenness show congruent spatial organization across a steep mountain gradient, or whether each metric captures a different dimension of ecological change.

The objectives of this study were to: (i) quantify plot-level alpha diversity and summarize richness along the sampled elevational gradient and among forest-type classes; (ii) describe community turnover using Bray-Curtis dissimilarity, non-metric multidimensional scaling (NMDS), and permutational multivariate analysis of variance (PERMANOVA); (iii) identify the principal environmental gradients in CCA; (iv) summarize indicator species, co-occurrence structure, and the SCI; and (v) describe plot-level and pixel-level EVI trends for 2000–2024.

2. Materials and Methods

2.1. Study area

The study was conducted across Bhutan, located in the eastern Himalaya, a region characterized by pronounced altitudinal gradients and diverse forest ecosystems. Vegetation data were derived from the National Forest Inventory (NFI), comprising species occurrence records from 1,942 georeferenced plots distributed across the country. The sampled plots span an elevation range of 113 to 5,469 m above sea level, with a mean elevation of 2,454.08 ± 1,271.20 m, capturing the full extent of ecological gradients from subtropical lowlands to alpine environments.

Bhutan’s forests were classified into 12 major forest-type classes: Blue Pine Forest, Chirpine Forest, Cool Broadleaved Forest, Dry Alpine Scrub, Evergreen Oak Forest, Fir Forest, Hemlock Forest, Juniper Rhododendron Scrub, Non-Forest, Spruce Forest, Subtropical Forest, and Warm

Broadleaved Forest. These classes represent dominant vegetation formations structured along climatic and elevational gradients. The spatial distribution of species richness across all inventory plots is presented in Fig. 1.

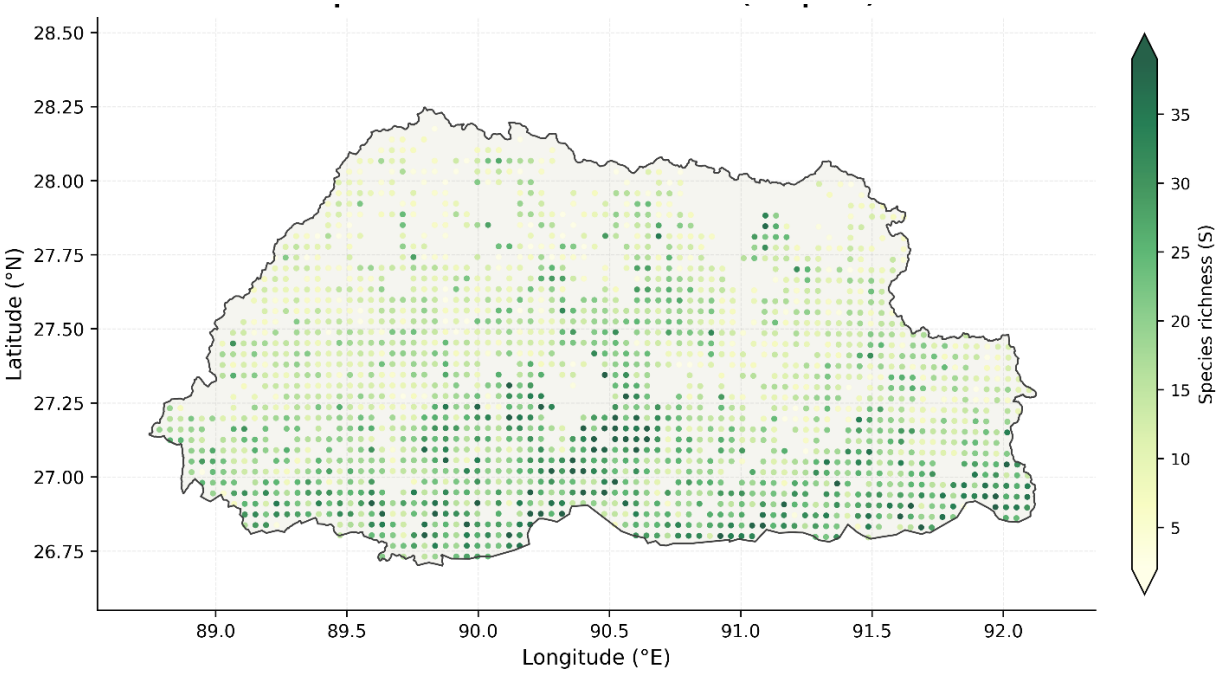

Fig. 1. Spatial distribution of species richness across 1,942 National Forest Inventory plots in Bhutan. Point size and colour represent plot-level species richness. Administrative boundaries are shown for reference and do not imply official delineation.

2.2. National Forest Inventory data and cleaning

Vegetation data were derived from the Bhutan National Forest Inventory (NFI, 2022). The dataset comprised species occurrence records stratified across three vertical vegetation layers: trees, shrubs, and herbs. The raw dataset contained 107,917 records, each associated with a plot identifier, geographic coordinates (longitude and latitude), species name, and corresponding local name. Across all records, 1,945 unique plot identifiers and 2,195 distinct non-empty species name entries were documented. The imported dataset retained the following fields: plot identifier, longitude, latitude, species name, and local name. In addition, sheet-specific count variables were included where available to preserve stratum-level abundance information.

Data preprocessing and cleaning were conducted using *pandas* (McKinney, 2010). Records were concatenated into a unified long-format table. Column names were standardized, leading and trailing whitespace was removed, and species-name strings were cleaned to ensure consistency. Geographic coordinates were parsed and validated, and records with missing plot identifiers or species names were excluded. The cleaned dataset comprised 107,876 records from 1,942 georeferenced plots and 2,185 unique, standardized species names. All records were verified to fall within the national extent of Bhutan based on the defined geographic bounds.

The cleaning workflow generated a taxonomic duplicate-candidate report; however, synonym resolution was not implemented automatically to avoid the introduction of unverified taxonomic assumptions. Furthermore, explicit height thresholds defining vertical strata were not recorded in

the field protocols. Therefore, vegetation strata were treated operationally according to the original NFI records classification (Trees, Shrubs, and Herbs) throughout the analysis.

2.3. Species matrix construction and environmental extraction

A species-by-plot matrix was constructed by aggregating records across all vegetation strata. Where an abundance field was available, values were converted to numeric, missing entries were replaced with 1, and abundance was summed by plot and species. Non-null abundance values occurred only in shrub records; consequently, tree and herb records contributed a single count per plot–species occurrence, whereas shrub records contributed observed abundance values where available. This differential treatment may introduce bias in abundance-sensitive metrics, including *Bray–Curtis* dissimilarity, by disproportionately weighting shrub composition.

The resulting dataset was structured in long format and subsequently aggregated for downstream analyses. Presence–absence information was retained for analyses insensitive to abundance, while abundance-weighted summaries were interpreted with caution given the underlying data structure. Environmental variables were extracted at plot centroids through point sampling of raster cell values using *rasterio* (Bunt et al., 2026). Elevation was obtained from the digital elevation model, and terrain derivatives (slope and aspect) were calculated using 3 × 3 moving windows. Bioclimatic variables (bio1–bio19) were derived from high-resolution (250 m) CMIP6 climate grids for Bhutan (Dorji et al., 2025).

Categorical variables were assigned using spatial joins. Forest type was attributed based on the nearest match to the national forest-type map, while soil type was extracted from the soil vector layer, with a raster-based fallback where necessary. The final environmental dataset comprised 1,942 plots spanning 12 forest-type classes. These environmental rasters represent spatially explicit proxies of vegetation–environment interactions commonly used in ecological analyses (Wang & Gamon, 2019). Summary statistics for all environmental variables included in the analysis are provided in Table S2.

2.4. Alpha diversity

Plot-level species richness, Shannon entropy, and Simpson diversity were calculated using *numpy* (Harris et al., 2020) and pandas. Stratum-specific richness for Trees, Shrubs, and Herbs was also computed. Richness was summarized by forest type and by nine 500-m elevation bands ranging from below 500 m to above 4,000 m (Fig. 2). Differences in richness among elevation bands were tested with the *Kruskal-Wallis test* (scipy.stats; Virtanen et al., 2020), and the effect size was quantified using $\varepsilon^2 = (H - k + 1)/(n - k)$, where H is the Kruskal-Wallis statistic, k is the number of groups, and n is the total sample size. This formula is epsilon-squared (ε^2; Tomczak & Tomczak, 2014), not eta-squared (η^2), and is reported as such throughout.

2.5. Beta diversity and community turnover

Bray-Curtis dissimilarity was calculated from the species matrix using *scipy.spatial.distance* (Virtanen et al., 2020), and a two-dimensional *Non-metric Multidimensional Scaling* (NMDS) was fitted using *sklearn.manifold.MDS* (Pedregosa et al., 2011) with a fixed random seed of 42 and 20 random initializations. Because the two-dimensional Kruskal stress-1 exceeded the commonly cited threshold of 0.30, a three-dimensional NMDS was also fitted with identical settings to assess whether adding a third axis substantially reduced stress. A supplementary *principal coordinates analysis* (PCoA) was also produced from the same dissimilarity matrix.

Compositional differences among forest-type classes were tested with Permutational Multivariate Analysis of Variance (PERMANOVA) *(skbio.stats.distance.permanova*;(Anderson & Walsh, 2013) using 999 permutations (Anderson, 2001). As a robustness check less sensitive to heterogeneous within-group dispersion, Analysis of Similarities (ANOSIM) was additionally computed using *skbio.stats.distance.anosim*; 999 permutations. As differences in dispersion can influence PERMANOVA results, within-group distances to centroids were compared among groups using Permutational Analysis of Multivariate Dispersion-distance-based test for homogeneity of group variances (PERMDISP2) (Anderson, 2006), providing a permutation-based F-test of homogeneity of multivariate dispersions. The PERMDISP test implementation is detailed in Supplementary Method SM3. To assess spatial autocorrelation in species composition, a Mantel test (Pearson method, 999 permutations) was applied between the Bray-Curtis dissimilarity matrix and a Haversine geographic-distance matrix; results are reported alongside PERMANOVA in Section 3.2. Details of the Mantel test implementation is provided in Supplementary Method SM1.

2.6. Canonical correspondence analysis

CCA was performed using *skbio.stats.ordination.cca* (Anderson & Walsh, 2013), following ter Braak (1986). The analysis retained the 200 most frequent species, removed plots that became all-zero after that filtering step, and fitted the ordination with 24 numeric environmental variables. Aspect was decomposed into northness *(sin[aspect])* and eastness *(cos[aspect])* before entry into the predictor matrix, replacing the raw degree value. Axis significance was assessed; 999 permutations per axis, conditioned on previously fitted axes. Grouped adjusted R^2 summaries were compiled for topographic (elevation, slope, aspect_northness, aspect_eastness) and climatic (bio1–bio19) predictor sets separately, following Borcard et al. (1992), including the shared and unexplained fractions. Variance inflation factors (VIF) were computed for all environmental variables using statsmodels (Seabold & Perktold, 2010) to diagnose collinearity among the bioclimatic predictors.

2.7. Indicator species analysis

Indicator-species analysis used an *IndVal-style* statistic (specificity × sensitivity) based on presence-absence, implemented in *numpy* and *pandas* (Dufrene & Legendre, 1997). Forest-type labels were permuted 999 times to evaluate significance. The analysis tested each species against each of its 12 forest-type classes independently (one test per species-type combination), resulting in up to 26,220 simultaneous tests. The resulting *p-values* were corrected for multiple testing using the Benjamini-Hochberg false discovery rate procedure (Benjamini & Hochberg, 1995) as implemented in *statsmodels* (Seabold & Perktold, 2010), applied across all species-type comparisons. Associations with FDR-adjusted $p \leq 0.05$ were reported as significant. The complete list of significant indicator species across all forest types is provided in Table S1.

2.8. Co-occurrence network analysis

The co-occurrence analysis binarized the species matrix, removed taxa occurring in fewer than three plots, and excluded ambiguous names (unknown, not listed, unidentified, or indeterminate). Species pairs were connected using a hypergeometric significance test per pair (hypergeom; Virtanen et al., 2020), controlling for marginal occupancies, with *False Discovery Rate (FDR)* correction applied across all tested pairs. The hypergeometric co-occurrence testing framework is described in Supplementary Method SM4. Network construction and community detection used

networkx (Hagberg et al., 2008) with the Louvain community detection algorithm (Blondel et al., 2008), which avoids the resolution limit of greedy modularity optimization.

Modularity was evaluated against a null model using repeated 2 × 2 checkerboard swaps (curveball algorithm) that preserved row and column marginal totals in the binary matrix. The analysis used 99 null permutations and reported observed modularity *Q*, standardized effect size *(SES*), and P(Q_null ≥ Q_obs).

2.9. Stratification Complexity Index (SCI)

The SCI was calculated directly from the alpha-diversity table, which contained per-plot richness, Shannon entropy, Simpson diversity (1−D), and stratum-specific richness for Trees, Shrubs, and Herbs. All six components were z-standardized using a safe z-score function (zero-standard-deviation columns set to zero) and summed to create the SCI. The SCI is interpreted here as a relative, plot-level composite summary for within-dataset comparison rather than as an absolute measure of vertical canopy layering. Leave-one-out sensitivity was assessed by omitting one z-standardized component at a time and correlating the reduced score with the full SCI using *scipy.stats.spearmanr*.

2.10. Spatially explicit Enhanced Vegetation Index (EVI) trend analysis

The remote-sensing analysis used precomputed MODIS MOD13Q1 rasters generated in Google Earth Engine, including a Theil–Sen slope raster, Mann–Kendall tau and p-value rasters, and an annual EVI composite stack spanning 2000–2024. EVI values are on the [0, 1] reflectance scale; a slope of 0.001 EVI yr^{-1} therefore corresponds to an increase of 0.01 EVI units per decade (Pettorelli et al., 2014). All raster sampling at plot coordinates used *rasterio* (Bunt et al., 2026). When the Mann–Kendall *p-value* band was entirely missing, p-values were derived analytically from tau using the normal approximation with continuity correction and tie-corrected variance (Mann, 1945), assuming 25 annual observations. The tie-corrected variance formulation for the Mann–Kendall test is provided in Supplementary Method SM5. Plot-level trends were classified at nominal $p \leq 0.05$, and pixel-level area statistics were reported under both nominal testing and Benjamini–Hochberg false discovery rate (FDR) correction, applied across 703,900 simultaneous pixel tests (Benjamini & Hochberg, 1995). The Theil–Sen estimator followed Sen (1968). Spearman rank correlations were calculated between plot-level EVI slope and both richness and SCI using *scipy.stats.spearmanr* (Virtanen et al., 2020).

2.11. Reproducibility

All analyses were executed in Python 3.12 through a modular workflow orchestrated by *python/run_pipeline.py*, which resolves dependencies across 14 analysis modules from data inspection and cleaning to final reporting. All stochastic procedures used a fixed seed of 42 throughout the workflow, including ordination *initialisation*, permutation tests, null-model simulations, network layout, and bootstrap resampling. Each run generated timestamped logs and a JSON run manifest with the execution order, input snapshot, cache status, and module outputs in *outputs/_run_logs/*, while module results were written to canonical archived tables and summaries under outputs/. All statistics reported below were taken directly from those archived output tables and summaries rather than recalculated manually. Code and documentation are available will made upon acceptance for publication.

3. Results

3.1. Alpha diversity along elevation and among forest types

The cleaned vegetation records retained 2,185 unique species across 1,942 plots. Mean plot richness was *17.09 ± 9.13* species, ranging from 1 to 57. Mean Shannon entropy (H') was *1.904 ± 0.661* and mean Simpson diversity (1−D) was *0.740 ± 0.190.* Mean stratum-specific richness was 9.14 ± 7.31 for Trees, 5.51 ± 4.20 for Shrubs, and 2.80 ± 3.17 for Herbs, indicating that most plot-level richness was concentrated in the tree and shrub strata. Because species richness is a non-negative right-skewed variable, mean ± SD should be interpreted alongside the medians reported in Table 1 rather than as a symmetric confidence interval.

Richness differed strongly among the nine elevation bands ($H = 630.801$, $p = 5.57 \times 10^{-131}$, $\varepsilon^2 = 0.3222$; Table 1). The highest mean richness occurred at 500–1,000 m (*24.83 ± 8.90 species; n = 172*), followed by the below-500 m band *(22.92 ± 10.41; n = 102).* Richness declined progressively through mid- and upper-elevation bands, reaching a minimum above 4,000 m *(8.86 ± 5.59; n = 285; Fig. 2).*

Table 1. Mean (±SD) and median species richness by 500-m elevation band. Kruskal-Wallis $H = 630.801$, $p = 5.57 \times 10^{-131}$, $\varepsilon^2 = 0.3222$ ($n = 9$ bands, $N = 1{,}942$ plots). Medians are provided as a supplement to means given the right-skewed distribution of species richness. The Total row is a summary row and is excluded from the statistical test; $k = 9$ elevation bands.

Elevation band (m)	*n* (plots)	Mean richness	SD	Median
<500	102	22.92	10.41	22.0
500–1,000	172	24.83	8.90	26.0
1,000–1,500	249	21.04	9.53	21.0
1,500–2,000	255	21.57	9.33	21.0
2,000–2,500	257	17.59	7.16	18.0
2,500–3,000	253	16.01	6.00	15.0
3,000–3,500	205	14.24	5.57	13.0
3,500–4,000	164	11.10	5.75	10.0
>4,000	285	8.86	5.59	8.0
Total	**1,942**	**17.09**	**9.13**	**16.0**

The same broad pattern was evident among forest-type classes (Table 2). Mean richness was highest in Subtropical Forest (*26.01 ± 8.70; n = 163*), Warm Broadleaved Forest (*24.23 ± 8.54; n = 376*), and Cool Broadleaved Forest (*18.55 ± 7.39; n = 301*), and lowest in Dry Alpine Scrub *(8.19 ± 4.74; n = 36),* Juniper Rhododendron Scrub *(10.70 ± 5.38; n = 57),* and Fir Forest *(11.33 ± 5.16; n = 206).*

Table 2. Forest-type summary: species richness, Stratification Complexity Index (SCI), and plot-level EVI trend statistics. Values are mean ± SD. EVI slope units are EVI yr^{-1} (EVI on [0, 1] scale). % Greening is the proportion of plots classified as significant greening at nominal $p \leq 0.05$. Forest types with $n < 30$ (marked †) have elevated uncertainty in SCI ranking.

Forest type	*n*	Mean richness ± SD	Mean SCI ± SD	Mean EVI slope	% Greening
Subtropical Forest	163	26.01 ± 8.70	3.13 ± 3.58	0.00153	62.58
Warm Broadleaved Forest	376	24.23 ± 8.54	2.80 ± 3.51	0.00164	58.78
Spruce Forest†	21	17.76 ± 5.05	1.39 ± 2.71	0.00010	0.00
Cool Broadleaved Forest	301	18.55 ± 7.39	0.66 ± 3.35	0.00112	38.21
Evergreen Oak Forest	179	17.27 ± 6.47	0.43 ± 2.96	0.00098	32.40
Blue Pine Forest	54	15.67 ± 5.18	0.15 ± 3.06	0.00026	16.67
Hemlock Forest	105	16.04 ± 6.28	0.09 ± 3.02	0.00082	24.76
Chirpine Forest	55	11.58 ± 7.13	−2.05 ± 3.95	0.00114	50.91
Fir Forest	206	11.33 ± 5.16	−2.06 ± 3.07	0.00047	12.14
Non-Forest	389	11.25 ± 7.49	−2.64 ± 4.45	0.00155	48.59
Juniper Rhododendron Scrub	57	10.70 ± 5.38	−2.94 ± 3.83	0.00120	42.11
Dry Alpine Scrub	36	8.19 ± 4.74	−4.25 ± 3.10	0.00147	38.89

Forest types with n < 30 have elevated uncertainty in SCI estimates.

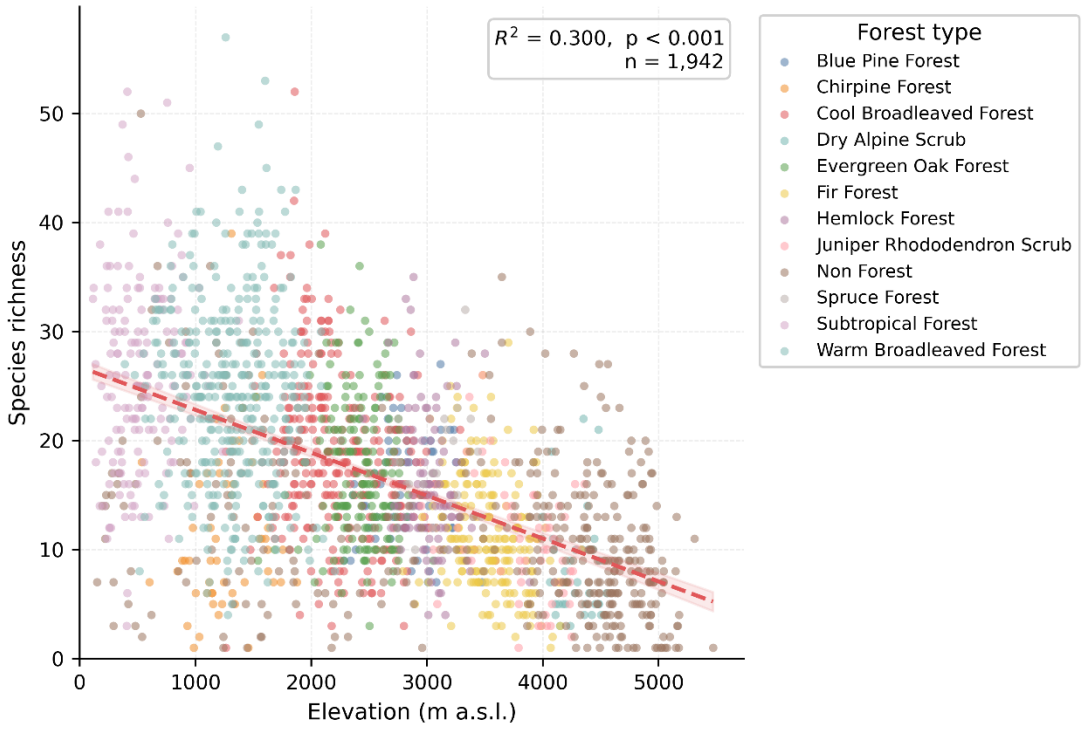

Fig. 2. Plot-level species richness against elevation. Points are coloured by joined forest-type class. The shaded band shows the 95% confidence interval around the locally fitted trend.

Pairwise post-hoc comparisons used Dunn's test with Benjamini-Hochberg FDR correction across 36 elevation-band pairs (scikit-posthocs, BH-FDR). The full Dunn's post-hoc testing procedure is described in Supplementary Method SM2. Of 36 unique pairs, 33 were significantly different after BH-FDR correction ($p < 0.05$). The three non-significant contrasts were all between contiguous low-elevation bands: <500 m vs. 1,000–1,500 m ($p = 0.287$), <500 m vs. 1,500–2,000 m ($p = 0.460$), and 1,000–1,500 m vs. 1,500–2,000 m ($p = 0.651$). The full pairwise matrix is reported in Supplementary Table S3.

3.2. Community turnover and forest-type differentiation

The two-dimensional NMDS returned a Kruskal stress-1 value of 0.3384 (Fig. 3), indicating that the ordination provides a poor low-dimensional representation of the underlying dissimilarity structure. A three-dimensional NMDS reduced stress to 0.2601, representing an improvement but still only a coarse approximation of community structure.

A supplementary (PCoA) based on the same Bray–Curtis dissimilarity matrix is provided as a metric complement to the NMDS (Fig. S1). Given the high dimensionality of the species dataset, the PCoA is presented for qualitative comparison only, and variance explained by individual axes is not interpreted.

Despite this ordination compression, forest type explained a statistically significant share of Bray–Curtis compositional variation in PERMANOVA (*pseudo-$F = 17.0279$, $R^2 = 0.0885$, $p = 0.001$; 999 permutations; $n = 1{,}942$; $k = 12$)*. The spatial distribution of the primary compositional gradient is illustrated in Fig. S2. ANOSIM confirmed the group separation (R = 0.356, p = 0.001; Clarke's (1993) scale: "barely separable to overlapping but distinguishable"), providing a result less sensitive to heterogeneous within-group dispersions.

PERMDISP2 (Anderson, 2006) confirmed heterogeneous multivariate dispersions among forest types (F = 58.91, p = 0.001; 999 permutations), indicating that the PERMANOVA result should be interpreted as reflecting both centroid separation and dispersion heterogeneity rather than differences in group location alone. The Mantel test revealed a weak but statistically significant association between Bray–Curtis dissimilarity and geographic distance (*Pearson $r = 0.0867$, $p = 0.001$; 999 permutations; $n = 1{,}942$*), indicating a weak distance–decay signal in species composition across the landscape.

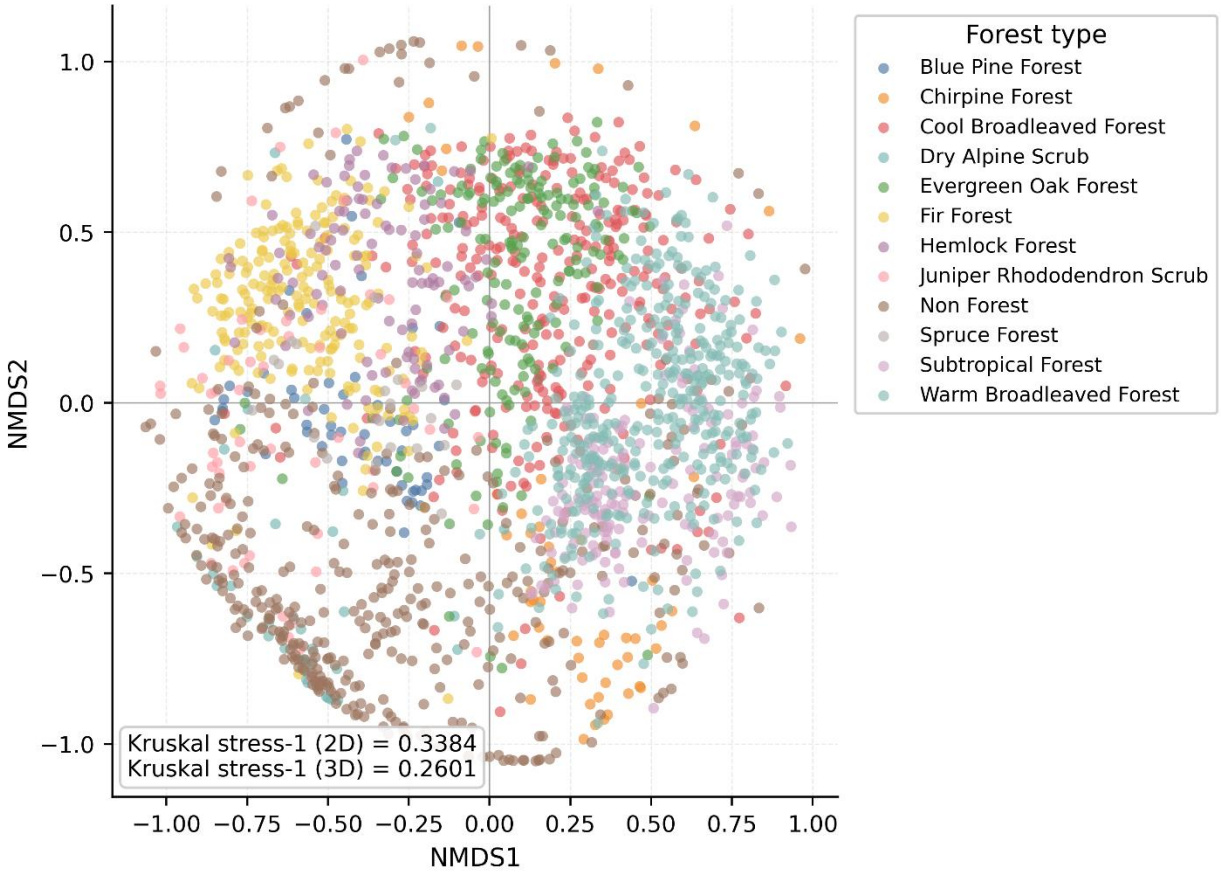

Fig. 3. Two-dimensional NMDS ordination of plot species composition based on Bray–Curtis dissimilarity (Kruskal stress-1 = 0.3384; three-dimensional solution: stress-1 = 0.2601). Points are coloured by joined forest-type class. The two-dimensional solution represents a poor low-dimensional fit, and the three-dimensional solution provides only a coarse approximation of community structure; patterns should therefore be interpreted with caution. A supplementary PCoA ordination is provided in Fig. S1 as a metric complement for qualitative comparison.

3.3. Environmental gradients in the constrained ordination

The CCA retained 1,915 plots, 200 species, and 24 environmental variables. CCA1 had an eigenvalue of 0.8728 and CCA2 had an eigenvalue of 0.4355. Both axes were significant at $p = 0.001$ (999 permutations, each axis conditioned on previously fitted axes; Fig. 4). The full constrained model had an adjusted $R^2 = 0.0422$. Variance inflation factor (VIF) diagnostics indicated extreme multicollinearity among several bioclimatic predictors ($VIF > 10^{13}$), precluding reliable interpretation of individual variable effects. Accordingly, the CCA results are interpreted at the level of composite environmental gradients rather than as independent contributions of specific predictors.

Environmental intra-set correlations (structure coefficients) indicated that CCA1 reflects a broad temperature–elevation gradient, characterized by strong correlations among multiple temperature-related variables (e.g., bio6, bio9, bio11, bio1) and elevation. CCA2 was associated with a precipitation-related gradient, with correlated contributions from several precipitation

variables (e.g., bio18, bio16, bio13, bio12). These variables should be interpreted as components of shared climatic gradients rather than as independent drivers of species composition.

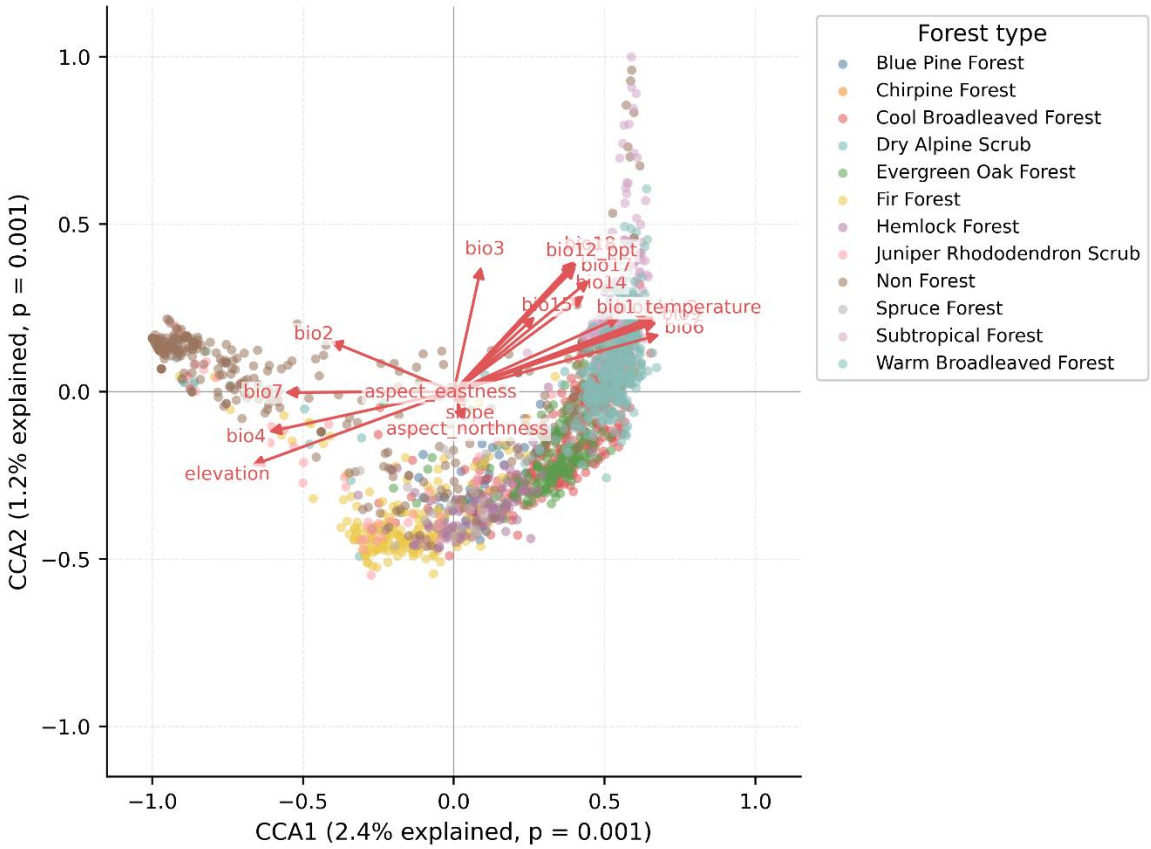

Fig. 4. Canonical correspondence analysis (CCA) site scores and environmental vectors for the retained 1,915 plots, 200 species, and 24 environmental variables. Both axes are significant at $p = 0.001$ (999 permutations). Arrow length is proportional to the strength of the environmental intra-set correlation. Several bioclimatic variables exhibit extreme collinearity *(VIF > 10^{13});* environmental vectors represent correlated gradients and should not be interpreted as independent effects.

Variance partitioning attributed adjusted $R^2 = 0.0136$ to topography (pure fraction 0.0026) and 0.0401 to climate (pure fraction 0.0291), with a shared topo–climate fraction of 0.011 and an unexplained fraction of 0.9573. Given the strong covariance among climatic predictors, these fractions should be interpreted as contributions of correlated environmental gradients rather than independent effects of specific variables.

3.4. Indicator species and co-occurrence structure

After Benjamini–Hochberg FDR correction, indicator analysis identified 162 significant species–forest type associations (FDR $p \leq 0.05$) across the 12 joined classes. The number of significant indicators was highest in Subtropical Forest (59) and remained comparatively large in Chirpine Forest (17), Spruce Forest (17), and Blue Pine Forest (15), whereas Cool Broadleaved Forest yielded only 1 and non-Forest yielded 1 (Table 3). The paucity of indicators for Cool Broadleaved Forest and non-Forest likely reflects their high compositional heterogeneity and

broad elevational ranges rather than analytical failure. High-scoring indicator species included *Pinus roxburghii* in Chirpine Forest (*IndVal = 0.7936, FDR p = 0.019*), *Picea spinulosa* in Spruce Forest (*0.4635, FDR p = 0.019*), *Pinus wallichiana* in Blue Pine Forest (*0.4111, FDR p = 0.019*), *Abies densa* in Fir Forest (*0.3870, FDR p = 0.019*), *Quercus lamellosa* in Evergreen Oak Forest (*0.3011, FDR p = 0.019*), *Pterospermum acerifolium* in Subtropical Forest (*0.3141, FDR p = 0.019*), and *Rhododendron anthopogon* in Dry Alpine Scrub (*0.2832, FDR p = 0.019*). All listed associations achieved the minimum permutation-based p-value (*p = 0.001; 999 permutations*); the corresponding Benjamini–Hochberg adjusted value for this rank is 0.019. The complete list of significant indicator species is provided in Table S1.

After filtering, the co-occurrence network contained 1,082 species nodes and 26,882 edges, with a mean degree of 49.69 (Fig. 5). Community detection using the Louvain algorithm (Blondel et al., 2008) identified four communities (*modularity Q = 0.3296*). Relative to a swap-based null model (99 permutations preserving species occupancy and plot-richness marginals), the observed modularity exceeded all null realizations (*p = 0.01; 99 permutations*). However, the standardized effect size was modest (SES = 1.415), indicating limited deviation from random expectations. Accordingly, the network should be interpreted as descriptive of co-occurrence structure rather than as evidence of strong ecological modularity. Edge weights represent shared-plot co-occurrence frequencies rather than direct ecological interactions. Selected high-confidence species co-occurrence associations are listed in Table S4.

Table 3. Top indicator species per forest-type class ranked by IndVal statistic. All associations significant at Benjamini-Hochberg FDR-corrected $p \leq 0.05$ (999 permutations). IndVal ranges from 0 to 1. All listed associations achieved the minimum permutation-based p-value (p = 0.001; 999 permutations); the Benjamini-Hochberg adjusted value for this rank is 0.019. Species names follow standard botanical nomenclature.

Forest type	**Top indicator species**	**IndVal**	**FDR *p***
Chirpine Forest	*Pinus roxburghii*	0.7936	0.019
Spruce Forest	*Picea spinulosa*	0.4635	0.019
Blue Pine Forest	*Pinus wallichiana*	0.4111	0.019
Fir Forest	*Abies densa*	0.3870	0.019
Subtropical Forest	*Pterospermum acerifolium*	0.3141	0.019
Evergreen Oak Forest	*Quercus lamellosa*	0.3011	0.019
Hemlock Forest	*Tsuga dumosa*	0.2860	0.019
Dry Alpine Scrub	*Rhododendron anthopogon*	0.2832	0.019
Warm Broadleaved Forest	*Maesa chisia*	0.1730	0.019
Juniper Rhododendron Scrub	*Juniperus recurva*	0.1017	0.019
Cool Broadleaved Forest	*Elatostema* sp.	0.0887	0.031
Non-Forest	*Saussurea* sp.	0.0810	0.019

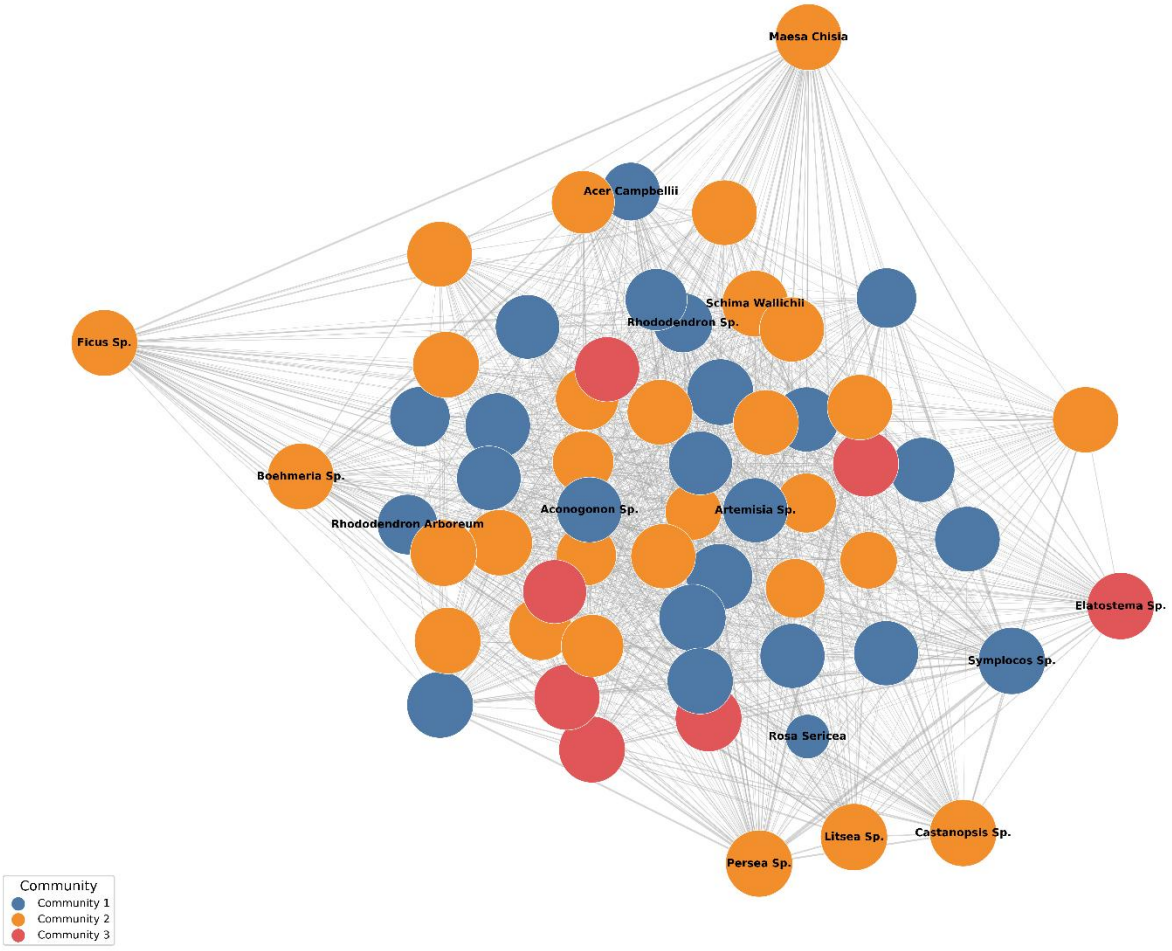

Fig. 5. Co-occurrence network for the top 60 species by degree extracted from the full network (*n = 1,082 species nodes; 26,882 edges*). Node size is proportional to species degree, and edge width represents shared-plot co-occurrence frequency. Community detection using the Louvain algorithm identified four communities (*modularity Q = 0.3296*). Observed modularity exceeded all values from the swap-based null model (*p = 0.01; 99 permutations*), but the standardized effect size (*SES = 1.415*) indicates only modest deviation from random expectations. The network should therefore be interpreted as descriptive of co-occurrence structure rather than evidence of strong ecological modularity. Edge weights represent co-occurrence frequencies and do not imply direct ecological interactions.

3.5. Stratification Complexity Index

The SCI ranged from *−11.85 to 16.68*, with mean near 0 and *SD = 4.22* (Fig. 6). The high SD relative to a sum of six z-standardized components (expected SD ≈ 2.45 if independent) indicates moderate inter-component correlation (*mean r ≈ 0.39*), reflecting the partial co-linearity of richness, Shannon entropy, Simpson diversity, and stratum-specific richness. Among the 12 forest-type classes, SCI was highest in Subtropical Forest (*3.13 ± 3.58; n = 163*), Warm Broadleaved Forest *(2.80 ± 3.51; n = 376)*, and Spruce Forest *(1.39 ± 2.71; n = 21; 95% CI: 0.21–2.57)*, and lowest in Dry Alpine Scrub *(−4.25 ± 3.10; n = 36; 95% CI: −5.26 to −3.24)*, Juniper Rhododendron Scrub *(−2.94 ± 3.83; n = 57)*, and Fir Forest *(−2.06 ± 3.07; n = 206)*.

The Spruce Forest and Dry Alpine Scrub rankings carry elevated uncertainty due to small sample sizes. The full forest-type SCI summary is reported in Table 2.

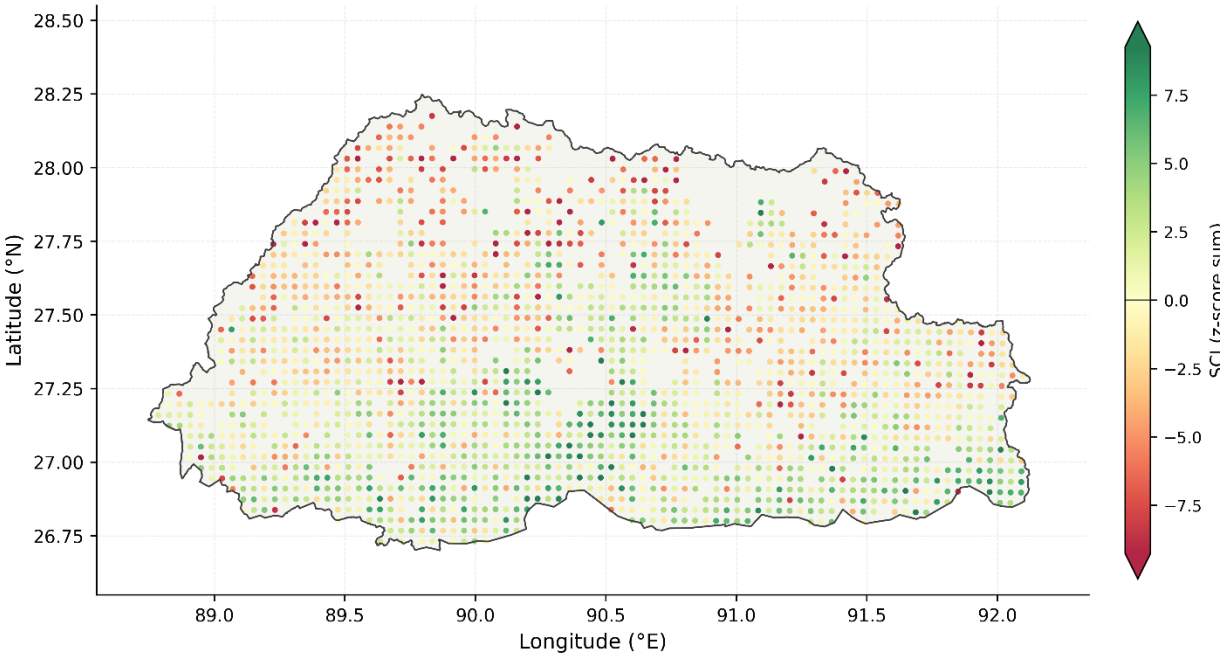

Fig. 6. Spatial distribution of the Stratification Complexity Index (SCI) across the 1,942 inventory plots in Bhutan. Map lines delineate study areas and do not necessarily depict accepted national boundaries.

Leave-one-out sensitivity analysis showed that index rankings were stable to the omission of any single z-standardized component. Spearman correlations between leave-one-out scores and the full SCI ranged from *0.9833 to 0.9980*, confirming that the composite score was not dominated by any single component.

3.6. EVI trend patterns across elevation and forest type

Pixel-level EVI area summaries showed widespread positive trends over 2000–2024 across 703,900 valid pixels (39,032.2 km²), with the estimated extent depending on the significance threshold applied (Table 4). Under the nominal threshold (*$p \leq 0.05$*), 298,245 pixels (*16,538.1 km²; 42.37% of valid raster area*) were classified as significant greening and 9,034 pixels (500.9 km²; 1.28%) as significant browning. After Benjamini–Hochberg FDR correction, the greening fraction declined to 210,180 pixels (*11,654.8 km²; 29.86%)* and the browning fraction to 5,076 pixels (*281.5 km²; 0.72%; Fig. 7*).

At the plot level, 811 plots were classified as Greening, 29 as Browning, and 1,102 as Stable. Mean EVI slope was highest below 500 m (*0.001870 EVI yr⁻¹; 70.59% significant greening*) and remained high at 500–1,000 m (*0.001661 EVI yr⁻¹; 62.21%*), while lower values were observed at higher elevations, including 3,000–3,500 m (*0.000639 EVI yr⁻¹; 22.44%)* and 3,500–4,000 m (*0.000610 EVI yr⁻¹; 18.90%;* Fig. 8).

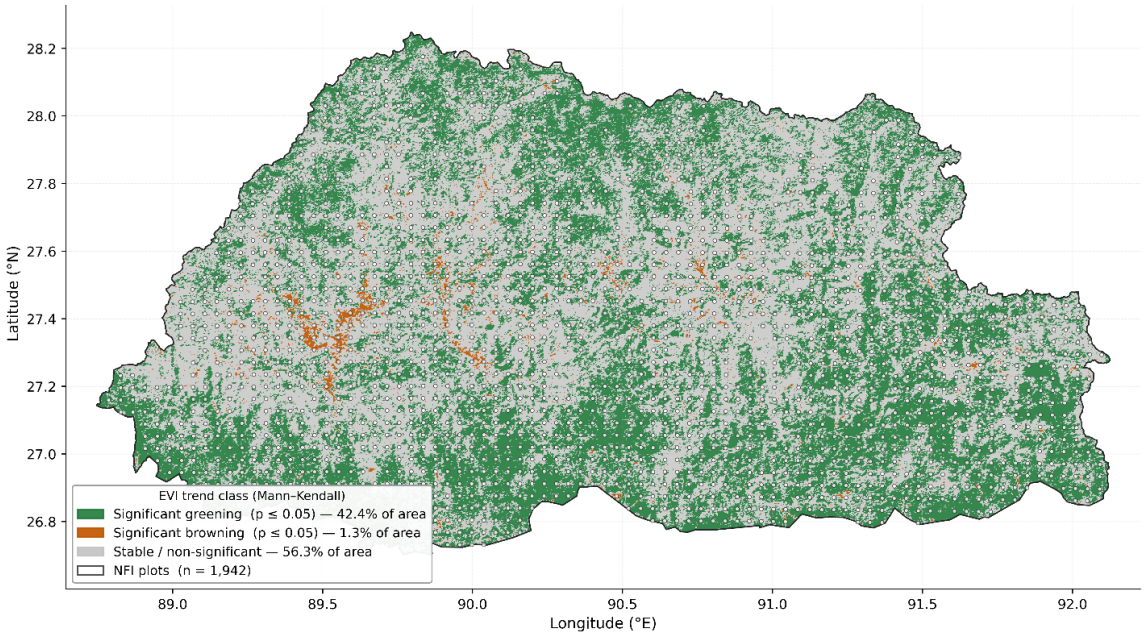

Fig. 7. Pixel-level MODIS EVI trend classification for 2000–2024 under the nominal Mann-Kendall threshold ($p \leq 0.05$). Map lines delineate study areas and do not necessarily depict accepted national boundaries.

Among forest types, Subtropical Forest (*62.58% significant greening; mean slope 0.001530 EVI yr⁻¹)* and Warm Broadleaved Forest (*58.78%; 0.001640 EVI yr⁻¹)* showed the highest proportions of greening. In contrast, Spruce Forest showed no significant *greening (0.00%; 0.000100 EVI yr⁻¹; n = 21),* which may reflect stable high-elevation canopy conditions. Fir Forest *(12.14%; 0.000470 EVI yr⁻¹)* and Blue Pine Forest (*16.67%; 0.000260 EVI yr⁻¹)* exhibited comparatively low levels of greening, indicating weak trends relative to other forest types (Table 4).

Table 4. Pixel-level MODIS EVI trend classification under nominal ($p \leq 0.05$) and Benjamini-Hochberg FDR-corrected thresholds. Total valid area = 703,900 pixels (39,032.2 km²). EVI on [0, 1] scale.

Threshold	Trend class	Pixels	Area (km²)	% of valid area
Nominal ($p \leq 0.05$)	Significant greening	298,245	16,538.1	42.37
	Significant browning	9,034	500.9	1.28
	Stable	396,621	21,993.2	56.35
FDR-corrected	Significant greening	210,180	11,654.8	29.86
	Significant browning	5,076	281.5	0.72
	Stable	488,644	27,095.9	69.42

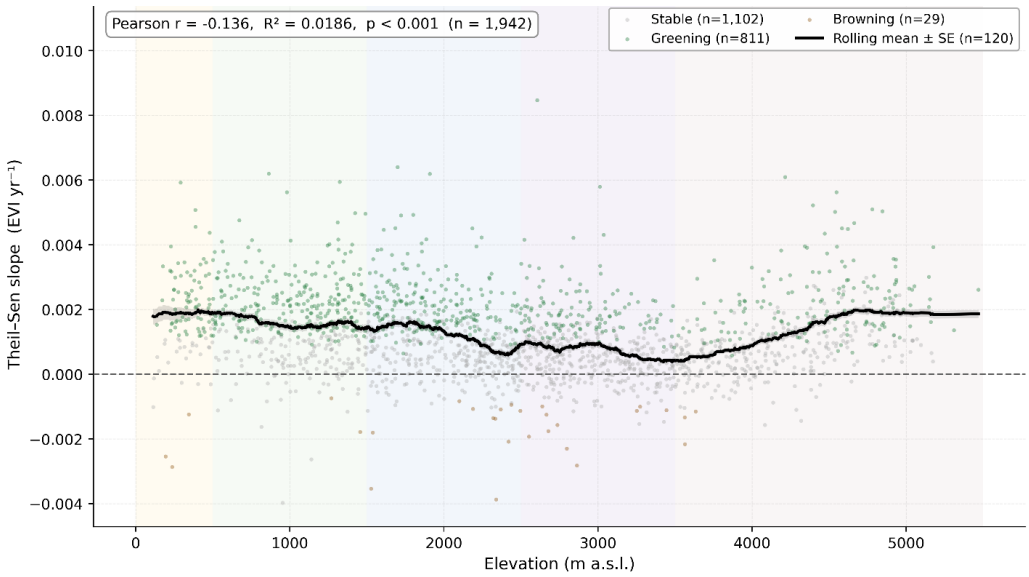

Fig. 8. Plot-level Theil-Sen EVI slope against elevation (m). Points represent individual inventory plots (*n* = 1,942) coloured by trend class (Greening, Stable, Browning).

Plot-level EVI slope showed weak but statistically significant positive correlations with species richness (*Spearman* $\rho = 0.1256$, $p = 2.80 \times 10^{-8}$; $\rho^2 = 0.0158$) and stratification complexity (SCI; $\rho = 0.0968$, $p = 1.95 \times 10^{-5}$; $\rho^2 = 0.0094$), indicating minimal association between remotely sensed greenness and plot-level biodiversity and structural complexity (Fig. 9).

EVI slope declined with elevation (*Spearman* $\rho = -0.1908$, $p = 2.20 \times 10^{-17}$), consistent with shorter growing seasons at higher altitudes. Spatial autocorrelation analysis (Moran's I) revealed significant positive clustering of EVI trends at short spatial lags *($I = 0.0395$, $z = 6.64$, $p < 0.001$ at ≈2.5 km*), which weakened at intermediate distances *($I = 0.0268$, $z = 2.29$, $p = 0.022$ at ≈10 km)* and became non-significant at ≈22 km *($I = 0.0297$, $z = 1.72$, $p = 0.085$)*, indicating locally coherent but spatially limited greening patterns.

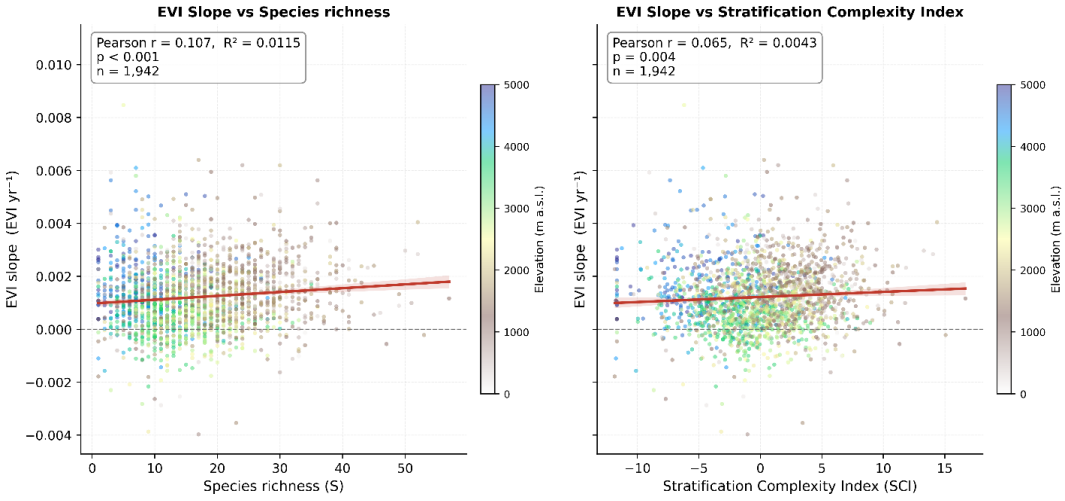

Fig. 9. Plot-level Theil-Sen EVI slope against species richness (left panel) and SCI (right panel). Lines show ordinary least-squares fit with 95% confidence interval (shown for visualization; OLS CI assumes homoscedastic residuals, which may not hold for these data). Spearman ρ = 0.1256 *(richness, $p = 2.80 \times 10^{-8}$) and $\rho = 0.0968$ (SCI, $p = 1.95 \times 10^{-5}$).*

4. Discussion

4.1. Elevational organization of richness and structural complexity

Species richness declined from lower to higher elevations across the sampled plots, with a peak at 500–1,000 m and a minimum above 4,000 m. The same directional pattern was evident among forest-type classes: Subtropical Forest and Warm Broadleaved Forest supported the highest richness (26.01 and 24.23 species per plot, respectively), whereas Dry Alpine Scrub and Juniper Rhododendron Scrub supported the lowest (8.19 and 10.70 species). The Stratification Complexity Index (SCI) exhibited the same broad organization, with highest mean values in low-elevation broadleaved classes and lowest values in high-elevation scrub systems.

Mechanistically, this pattern is consistent with elevation-driven environmental filtering, in which temperature, growing-season length, and resource availability decline with altitude, constraining both species persistence and vertical vegetation development. Lower elevations therefore support larger regional species pools and greater niche packing, while also enabling the coexistence of multiple vegetation strata through reduced climatic limitation. This joint response of diversity and structural organization reflects the coupling of productivity gradients and life-form diversification in mountain ecosystems (Lomolino, 2001; McCain, 2009). Beyond the focal landscape, the observed co-variation of richness and structural complexity is consistent with patterns reported across climatically stratified mountain systems globally, including the Andes and temperate alpine regions, where thermal constraints and energy availability jointly structure biodiversity and vegetation architecture. However, the strength of this relationship in the present dataset also reflects the construction of SCI as a composite index integrating richness, diversity, and stratum-specific components.

Accordingly, SCI should be interpreted as an operational summary of structural–diversity organization rather than an independent measure of canopy stratification. Because total richness is partly decomposed into stratum-specific richness components, SCI contains internally redundant information and is best understood as a relative indicator for within-dataset comparison. Its value lies in providing a reproducible, inventory-scale metric that captures multi-stratum vegetation organization in the absence of direct structural measurements, rather than as a standalone ecological property transferable across systems without validation.

Even with this constraint, the coincidence of high richness and high SCI in lower-elevation broadleaved forests suggests that the most biodiverse portions of mountain gradients also tend to support the most structurally complex vegetation assemblages, reflecting the joint influence of favourable climatic conditions and reduced environmental filtering. From a management perspective, this implies that low-elevation forest belts may represent disproportionate concentrations of ecological value, combining high species diversity, complex vertical structure, and increased exposure to anthropogenic pressures due to accessibility. Prioritizing these zones for monitoring and retention is therefore likely to yield the greatest conservation returns in mountain landscapes.

4.2. Forest-type differentiation and environmental sorting

The turnover and ordination analyses indicate that forest-type classes capture real but incomplete compositional structure. PERMANOVA detected significant differences among the 12 joined forest classes, yet the explained fraction was modest *($R^2 = 0.0885$),* the two-dimensional NMDS stress was high (0.3384), and dispersion also differed significantly among groups. Three-dimensional NMDS reduced stress to 0.2601, which still indicates poor fit; both values point to high intrinsic dimensionality in the Bray–Curtis dissimilarity structure that no low-dimensional projection can fully represent. The ANOSIM result *($R = 0.356$, $p = 0.001$*; Clarke's scale: "barely separable") corroborates the significant group differentiation while being less sensitive to the unequal within-group dispersions. The CCA results are consistent with this picture: climate *(adjusted $R^2 = 0.0401$*) explained more compositional variation than topography (*adjusted $R^2 = 0.0132$),* but the full model explained only a small fraction of total variation *(adjusted $R^2 = 0.0422$).* The severe collinearity among bioclimatic variables *(VIF > 10^{13} for bio5, bio6, and bio7)* prevents independent attribution of effects to individual temperature variables. Taken together, these results indicate that climate as a whole structures community composition, but only partially, within a high-dimensional ecological system (Zarnetske et al., 2019).

The apparent tension between the modest PERMANOVA R^2 (8.85% of overall variation explained by forest type) and the 162 significant indicator species is ecologically consistent rather than contradictory. PERMANOVA integrates signal across all 200+ species simultaneously, where species-specific associations are diluted by the many species with weak forest-type fidelity. Indicator-species analysis, by contrast, tests each species individually against specific forest-type classes, detecting associations even when the overall multivariate signal is weak. The coexistence of weak global differentiation and strong individual-species associations is therefore a genuine ecological feature of this system, not an artefact.

Taken together, these outputs support a broader inference relevant to mountain forest classification: mapped forest types usually capture genuine climatic sorting, but they remain coarse summaries of ecologically heterogeneous assemblages. For international applications, forest-type maps are useful starting points for stratification and reporting, but should be paired with plot-based compositional analyses when management depends on fine-scale floristic turnover.

4.3. Indicator taxa, network structure, and interpretation

After Benjamini-Hochberg FDR correction across 2,185 species, 162 associations remained significant, a reduction from 416 at the uncorrected threshold that reflects the large number of simultaneous tests rather than weak floristic differentiation. The retained associations were concentrated in Subtropical Forest (59 indicators), Chirpine Forest (17), and Spruce Forest (17), which are structurally and climatically distinctive forest classes. The strong indicator species such as *Pinus roxburghii* in Chirpine Forest, *Picea spinulosa* in Spruce Forest, *Abies densa* in Fir Forest, and *Rhododendron anthopogon* in Dry Alpine Scrub—confirm that the joined forest classes retain recognizable floristic identities despite the modest global effect sizes from PERMANOVA and CCA.

The network results require cautious interpretation: although modularity exceeded null expectations (*SES = 1.415, $p = 0.01$; 99 permutations*), the effect size was modest, and the underlying edges represent shared plot occupancy rather than ecological interactions. Indicator-

species analysis therefore offers a more management-ready basis for interpretation than co-occurrence network structure when null-model support is weak.

4.4. Greenness trends and their correspondence with diversity summaries

The EVI analyses indicate widespread positive vegetation trends over 2000–2024, but the magnitude of the greening signal depends strongly on how statistical significance is defined. Nominal testing classified 42.37% of the valid raster area as greening, whereas the Benjamini–Hochberg false discovery rate (FDR)-corrected estimate was 29.86%. This discrepancy highlights the sensitivity of large-area inference to multiple-testing control and indicates that uncorrected estimates substantially overstate the spatial extent of greening. Accordingly, both values are informative, but the FDR-corrected estimate provides a more conservative and robust basis for interpretation at landscape scale.

Greening patterns were not spatially uniform. Lower-elevation bands and low-elevation forest types exhibited the highest proportions of significant greening, whereas several high-elevation conifer systems showed weaker or negligible trends. This elevational gradient in greenness is consistent with declining temperature and growing-season length, which constrain productivity at higher elevations and limit the magnitude of detectable vegetation change. However, interpretation of EVI trends in mountain systems requires careful consideration of multiple confounding processes that can decouple greenness from underlying ecological condition.

Several mechanisms are likely to contribute to the observed spatial patterns. At lower elevations, land-use change and secondary forest recovery, including regrowth on abandoned agricultural land, can generate strong positive greenness trends without corresponding increases in native biodiversity or structural integrity (Pettorelli et al., 2014). At higher elevations, shrub expansion near treelines can increase canopy greenness while simultaneously altering species composition and reducing herbaceous diversity (Myers-Smith et al., 2011). In addition, snow cover and seasonal persistence of snowpack can suppress or distort optical vegetation indices, complicating the interpretation of interannual trends in alpine environments (Pettorelli et al., 2014). Atmospheric effects, including aerosol loading, may further influence reflectance signals, although their contribution to long-term EVI trends remains context dependent. Together, these processes indicate that greenness trends integrate multiple ecological and non-ecological signals, limiting their interpretability as direct indicators of ecosystem condition. At the plot level, EVI slope was positively associated with both species' richness and SCI, but the relationships were weak ($\rho = 0.1256$ *and* $\rho = 0.0968$, *respectively*), indicating that long-term changes in canopy greenness capture only a small fraction of the variation in biodiversity and structural complexity. Although statistically significant, these correlations are ecologically negligible in magnitude and demonstrate that productivity-related signals derived from satellite data are only loosely coupled to compositional and structural attributes measured in field inventories.

This weak coupling has broader implications for ecological monitoring in mountain systems. It suggests that remotely sensed greenness cannot be treated as a reliable proxy for biodiversity or structural complexity, even across strong environmental gradients. Instead, greenness metrics should be interpreted as complementary indicators that provide information on canopy dynamics and productivity, but require integration with plot-based data to support robust ecological inference. For monitoring programs in other mountain landscapes, this implies that reliance on single-indicator frameworks will systematically underrepresent ecosystem dynamics, and that

multi-indicator approaches combining remote sensing with field-based composition and structure data are necessary to capture the full complexity of ecological change (Schweiger et al., 2018; Pettorelli et al., 2014; Kacic & Kuenzer, 2022; Muise et al., 2024).

4.5. Transferability, methodological constraints, and priorities for future work

This study demonstrates a transferable analytical framework for integrating national forest inventories with environmental data and long-term remote sensing in mountain systems. Three principles emerge as broadly applicable. First, inventory plots, environmental extraction, multivariate community analyses, indicator-species tests, structural summaries, and time-series remote sensing are most informative when analyzed as a linked, multi-component system, rather than as independent metrics. Second, broad forest classifications and remotely sensed greenness layers are useful for screening and stratification, but do not substitute for plot-based compositional data when ecological specificity is required for conservation or restoration decisions. Third, reproducible, script-based workflows enable this integration to be implemented consistently at management scale, providing a traceable and repeatable baseline for longitudinal monitoring (Pereira et al., 2013; Cavender-Bares et al., 2022).

Beyond these operational lessons, the results support a more general inference relevant to mountain monitoring frameworks: single-indicator approaches are insufficient to characterize ecological change in heterogeneous, climate-stratified systems. The weak coupling observed between greenness, diversity, and structural complexity implies that monitoring programs relying on any one of these dimensions in isolation will systematically underrepresent ecosystem dynamics. Integrated, multi-indicator designs are therefore not only advantageous but necessary for valid ecological inference in mountain landscapes.

Several methodological constraints warrant explicit acknowledgment. First, abundance information is unevenly represented across strata: shrub records include quantitative counts, whereas tree and herb records are recorded primarily as presence observations. This imbalance can influence abundance-sensitive metrics such as *Bray–Curtis* dissimilarity and complicate direct comparisons among strata. Second, although the data-cleaning workflow flags potential duplicate species names, it does not implement automated synonym resolution, which may introduce residual taxonomic inconsistency in species-level analyses. In addition, the Stratification Complexity Index (SCI) aggregates multiple diversity and stratum-specific components and therefore incorporates partially redundant information; it should be interpreted as an operational composite index rather than a formally validated measure of structural complexity, and its transferability across ecological systems remains to be established through independent validation.

Two analytical limitations warrant particular attention. The high stress values observed in both two-dimensional (0.3384) and three-dimensional (0.2601) NMDS solutions indicate that the underlying compositional structure is inherently high-dimensional and cannot be adequately represented in low-dimensional ordination space. Ordination outputs should therefore be interpreted as approximate visual summaries rather than precise representations of ecological distance. Additionally, extreme collinearity among bioclimatic variables (VIF > 10^{13}) limits the ability of canonical correspondence analysis to attribute compositional variation to individual predictors. The CCA results provide robust evidence that climate as a composite gradient

structures community composition, but do not support independent inference regarding specific temperature or precipitation variables.

Future work should address these limitations through (i) variable selection or dimensionality reduction of climatic predictors prior to constrained ordination, (ii) harmonization of abundance information across vegetation strata, (iii) automated taxonomic standardization to reduce synonym-related uncertainty, and (iv) independent validation of structural metrics, including comparison of SCI with field-based or remotely sensed canopy structure data such as LiDAR. Extending this framework across multiple re-inventory cycles and contrasting mountain regions would further enable evaluation of the temporal stability and geographic generality of the patterns identified here.

5. Conclusions

This study delivers a national-scale, integrative assessment of mountain forest organization in Bhutan by explicitly linking species diversity, community turnover, structural complexity, and long-term canopy dynamics across a full elevational gradient. The results show that these dimensions form coherent but only partially coupled patterns: richness and structural complexity decline sharply with elevation, low-elevation broadleaved systems concentrate both diversity and vertical complexity, and forest-type classes capture meaningful yet incomplete compositional differentiation. Indicator-species analysis provides operationally robust, class-specific associations, while community analyses reveal a high-dimensional structure governed by overlapping environmental gradients rather than discrete ecological boundaries. In contrast, MODIS EVI trends indicate widespread greening over 2000–2024, but their weak association with plot-based diversity and structure demonstrates that canopy greenness is not a reliable proxy for underlying ecological condition.

These findings have direct implications for policy and monitoring. First, single-indicator approaches—especially those relying on satellite greenness—risk systematic misinterpretation of ecosystem change and should be complemented with field-based biodiversity and structural metrics. Second, low-elevation forests emerge as priority systems where high ecological value coincides with greater anthropogenic pressure, reinforcing their importance for conservation and climate-adaptation planning. Third, the elevational baseline established here supports vertically connected management strategies that reflect continuous environmental gradients rather than rigid forest-type boundaries. Methodologically, the study provides a reproducible, scalable framework that integrates inventory data, multivariate community ecology, structural indices, and remote sensing into a unified monitoring system applicable to mountain regions globally. At the same time, it identifies clear priorities for improvement, including harmonization of abundance data across strata, rigorous taxonomic standardization, reduction of collinearity among environmental predictors, and independent validation of composite structural indices. Overall, effective monitoring and management of climate-sensitive mountain forests require explicitly multi-dimensional approaches in which biodiversity, structure, and canopy dynamics are jointly evaluated rather than treated as interchangeable signals of ecological change.

CRediT authorship contribution statement

Wangdi: Conceptualization, Methodology, Software, Formal analysis, Data curation, Visualization, Writing – original draft, Writing – review & editing, Project administration.

Laxmi Sagar: Methodology, Formal analysis, Validation, Writing – review & editing.

Sangay Chedup: Data curation, Field investigation, Writing – review & editing.

Sangay Dorjee: Data validation, Writing – review & editing.

Tashi Waiba Norbu: Supervision, Writing – review & editing.

Declaration of competing interest

The authors declare that they have no known competing financial interests or personal relationships that could have appeared to influence the work reported in this paper.

Declaration of generative AI and AI-assisted technologies in the writing process

During the preparation of this work the authors used AI-assisted tools to support language editing and manuscript structuring. After using these tools, the authors reviewed and edited the content as needed and take full responsibility for the content of the published article.

Data availability

The processed vegetation and environmental data, analysis code, and generated outputs supporting this article will be made available from the corresponding author on reasonable request. The raw National Forest Inventory data are owned by the Department of Forests and Park Services, Bhutan, and are subject to institutional data-sharing arrangements.

Acknowledgements

The authors acknowledge the Department of Forests and Park Services, Bhutan, for providing National Forest Inventory data. We also thank the MODIS Land Team for MOD13Q1 EVI products and Google Earth Engine for supporting geospatial processing of the remote-sensing inputs used in this study.

Funding

This research did not receive any specific grant from funding agencies in the public, commercial, or not-for-profit sectors.

References

Anderson, M. J. (2001). A new method for non-parametric multivariate analysis of variance. *Austral Ecology, 26(1)*, 32–46. https://doi.org/10.1046/j.1442-9993.2001.01070.x

Anderson, M. J. (2006). Distance-based tests for homogeneity of multivariate dispersions. *Biometrics, 62(1)*, 245–253. https://doi.org/10.1111/j.1541-0420.2005.00440.x

Anderson, M. J., & Walsh, D. C. I. (2013). *PERMANOVA, ANOSIM, and the Mantel test in the face of heterogeneous dispersions: What null hypothesis are you testing? Ecological Monographs, 83(4)*, 557–574. https://doi.org/10.1890/12-2010.1

Benjamini, Y., & Hochberg, Y. (1995). Controlling the false discovery rate: A practical and powerful approach to multiple testing. *Journal of the Royal Statistical Society: Series B, 57(1)*, 289–300. https://doi.org/10.1111/j.2517-6161.1995.tb02031.x

Blondel, V. D., Guillaume, J.-L., Lambiotte, R., & Lefebvre, E. (2008). Fast unfolding of communities in large networks. *Journal of Statistical Mechanics: Theory and Experiment, 2008(10)*, P10008. https://doi.org/10.1088/1742-5468/2008/10/P10008

Borcard, D., Legendre, P., & Drapeau, P. (1992). Partialling out the spatial component of ecological variation. *Ecology, 73(3)*, 1045–1055. https://doi.org/10.2307/1940179

Bunt, F., Johnson, J., & Hogland, J. (2026). Raster Tools: An open-source toolbox for raster processing. *Journal of Open-Source Software, 11(119)*, 8134. https://doi.org/10.21105/joss.08134

Cavender-Bares, J., Gamon, J. A., Hobbie, S. E., Madritch, M. D., Meireles, J. E., Schweiger, A. K., & Townsend, P. A. (2022). Integrating remote sensing with ecology and evolution to advance biodiversity conservation. *Nature Ecology & Evolution, 6(4)*, 506–519. https://doi.org/10.1038/s41559-022-01702-5

Clarke, K. R. (1993). Non-parametric multivariate analyses of changes in community structure. *Australian Journal of Ecology, 18(1)*, 117–143. https://doi.org/10.1111/j.1442-9993.1993.tb00438.x

Dorji, S., Stewart, S., Bajwa, A., Aziz, A., Shabbir, A., & Adkins, S. (2025). High-resolution (250 m) historical and projected (CMIP6) air temperature and precipitation grids for Bhutan (Version 1) [Data set]. CSIRO. https://doi.org/10.25919/pec2-hs50

Dufrêne, M., & Legendre, P. (1997). Species assemblages and indicator species: The need for a flexible asymmetrical approach. *Ecological Monographs, 67(3)*, 345–366. https://doi.org/10.1890/0012-9615(1997)067[0345:SAAIST]2.0.CO;2

Hagberg, A. A., Schult, D. A., & Swart, P. J. (2008). Exploring network structure, dynamics, and function using NetworkX. In G. Varoquaux, T. Vaught, & J. Millman (Eds.), Proceedings of the 7th Python in Science Conference (pp. 11–15).

Harris, C. R., Millman, K. J., van der Walt, S. J., Gommers, R., Virtanen, P., Cournapeau, D., & Oliphant, T. E. (2020). Array programming with NumPy. *Nature, 585*, 357–362. https://doi.org/10.1038/s41586-020-2649-2

Kacic, P., & Kuenzer, C. (2022). Forest biodiversity monitoring based on remotely sensed spectral diversity: A review. *Remote Sensing, 14(21)*, 5363. https://doi.org/10.3390/rs14215363

Körner, C. (2007). The use of "altitude" in ecological research. *Trends in Ecology & Evolution, 22(11)*, 569–574. https://doi.org/10.1016/j.tree.2007.09.006

Lomolino, M. V. (2001). Elevation gradients of species-density: Historical and prospective views. *Global Ecology and Biogeography, 10(1)*, 3–13. https://doi.org/10.1046/j.1466-822X.2001.00229.x

Mann, H. B. (1945). Nonparametric tests against trend. *Econometrica, 13(3)*, 245–259. https://doi.org/10.2307/1907187

Mantel, N. (1967). The detection of disease clustering and a generalized regression approach. *Cancer Research, 27*, 209–220.

McCain, C. M. (2009). Global analysis of bird elevational diversity. *Global Ecology and Biogeography, 18(3)*, 346–360. https://doi.org/10.1111/j.1466-8238.2008.00443.x

McKinney, W. (2010). Data structures for statistical computing in Python. In Proceedings of the 9th Python in Science Conference (pp. 56–61).

Mountain Research Initiative EDW Working Group. (2015). Elevation-dependent warming in mountain regions of the world. *Nature Climate Change, 5*, 424–430. https://doi.org/10.1038/nclimate2563

Muise, E. R., Andrew, M. E., Coops, N. C., Wulder, M. A., White, J. C., Hermosilla, T., & others. (2024). Disentangling linkages between satellite-derived indicators of forest structure and productivity for ecosystem monitoring. *Scientific Reports, 14*, 13717. https://doi.org/10.1038/s41598-024-64615-2

Myers, N., Mittermeier, R. A., Mittermeier, C. G., da Fonseca, G. A. B., & Kent, J. (2000). Biodiversity hotspots for conservation priorities. *Nature, 403*, 853–858. https://doi.org/10.1038/35002501

Myers-Smith, I. H., Forbes, B. C., Wilmking, M., Hallinger, M., Lantz, T., Blok, D., Tape, K. D., Macias-Fauria, M., Sass-Klaassen, U., Lévesque, E., Boudreau, S., Ropars, P., Hermanutz, L., Trant, A., Collier, L. S., Weijers, S., Rozema, J., Rayback, S. A., Schmidt, N. M., & Hik, D. S. (2011). Shrub expansion in tundra ecosystems: Dynamics, impacts and research priorities. *Environmental Research Letters, 6(4)*, 045509. https://doi.org/10.1088/1748-9326/6/4/045509

Pedregosa, F., Varoquaux, G., Gramfort, A., Michel, V., Thirion, B., Grisel, O., & Duchesnay, É. (2011). Scikit-learn: Machine learning in Python. *Journal of Machine Learning Research*, *12*, 2825–2830.

Pereira, H. M., Ferrier, S., Walters, M., Geller, G. N., Jongman, R. H. G., Scholes, R. J., Bruford, M. W., Brummitt, N., Butchart, S. H. M., Cardoso, A. C., Coops, N. C., Dulloo, E., Faith, D. P., Freyhof, J., Gregory, R. D., Heip, C., Höft, R., Hurtt, G., Jetz, W., & Wegmann, M. (2013). Essential biodiversity variables. *Science, 339(6117)*, 277–278. https://doi.org/10.1126/science.1229931

Pettorelli, N., Laurance, W. F., O'Brien, T. G., Wegmann, M., Nagendra, H., & Turner, W. (2014). Satellite remote sensing for applied ecologists: Opportunities and challenges. *Journal of Applied Ecology, 51(4)*, 839–848. https://doi.org/10.1111/1365-2664.12261

Schweiger, A. K., Cavender-Bares, J., Townsend, P. A., Hobbie, S. E., Madritch, M. D., Wang, R., Tilman, D., & Gamon, J. A. (2018). Plant spectral diversity integrates functional and phylogenetic components of biodiversity and predicts ecosystem function. *Nature Ecology & Evolution, 2(6)*, 976–982. https://doi.org/10.1038/s41559-018-0551-1

Seabold, S., & Perktold, J. (2010). Statsmodels: Econometric and statistical modeling with Python. In Proceedings of the 9th Python in Science Conference (pp. 92–96). https://doi.org/10.25080/Majora-92bf1922-011

Sen, P. K. (1968). Estimates of the regression coefficient based on Kendall's tau. *Journal of the American Statistical Association, 63(324)*, 1379–1389. https://doi.org/10.1080/01621459.1968.10480934

Skidmore, A. K., Coops, N. C., Neinavaz, E., Ali, A., Schaepman, M. E., Paganini, M., Kissling, W. D., Vihervaara, P., Darvishzadeh, R., Feilhauer, H., Fernandez, M., Fernández, N., Gorelick, N., Geijzendorffer, I., Heiden, U., Heurich, M., Hobern, D., Holzwarth, S., Muller-Karger, F. E., & Wingate, V. (2021). Priority list of biodiversity metrics to observe from space. *Nature Ecology & Evolution, 5*, 896–906. https://doi.org/10.1038/s41559-021-01451-x

ter Braak, C. J. F. (1986). Canonical correspondence analysis: A new eigenvector technique for multivariate direct gradient analysis. *Ecology, 67(5)*, 1167–1179. https://doi.org/10.2307/1938672

Tomczak, M., & Tomczak, E. (2014). The need to report effect size estimates revisited: An overview of some recommended measures of effect size. *Trends in Sport Sciences, 21(1)*, 19–25.

Virtanen, P., Gommers, R., Oliphant, T. E., Haberland, M., Reddy, T., Cournapeau, D., & van der Walt, S. J. (2020). SciPy 1.0: Fundamental algorithms for scientific computing in Python. *Nature Methods, 17*, 261–272. https://doi.org/10.1038/s41592-019-0686-2

Wang, R., & Gamon, J. A. (2019). Remote sensing of terrestrial plant biodiversity. *Remote Sensing of Environment, 231*, 111218. https://doi.org/10.1016/j.rse.2019.111218

Wangda, P., & Ohsawa, M. (2006). Structure and regeneration dynamics of dominant tree species along altitudinal gradients in the dry valley slopes of the Bhutan Himalaya. *Forest Ecology and Management, 230*(1–3), 136–150. https://doi.org/10.1016/j.foreco.2006.04.019

Zarnetske, P. L., Read, Q. D., Record, S., Gaddis, K. D., Pau, S., Hobi, M. L., Malone, S. L., Costanza, J., Dahlin, K. M., Latimer, A. M., Wilson, A. M., Grady, J. M., Ollinger, S. V., & Finley, A. O. (2019). Towards connecting biodiversity and geodiversity across scales with satellite remote sensing. *Global Ecology and Biogeography, 28(5)*, 548–556. https://doi.org/10.1111/geb.12887